Synthetic and Systems Biotechnology 8 (2023) 386–395

Contents lists available at ScienceDirect

Synthetic and Systems Biotechnology

journal homepage: www.keaipublishing.com/en/journals/synthetic-and-systems-biotechnology

Directed evolution of a neutrophilic and mesophilic methanol dehydrogenase based on high-throughput and accurate measurement of formaldehyde

Jin Qian [a,c,1], Liwen Fan [c,1], Jinxing Yang [f], Jinhui Feng [c], Ning Gao [c,e], Guimin Cheng [a,c], Wei Pu [c], Wenjuan Zhou [c], Tao Cai [c], Shuang Li [f], Ping Zheng [c,d,e], Jibin Sun [c,d,e], Depei Wang [a,**], Yu Wang [a,b,c,d,e,*]

[a] College of Biotechnology, Tianjin University of Science and Technology, Tianjin, 300222, China
[b] Haihe Laboratory of Synthetic Biology, Tianjin, 300308, China
[c] Key Laboratory of Engineering Biology for Low-carbon Manufacturing, Tianjin Institute of Industrial Biotechnology, Chinese Academy of Sciences, Tianjin, 300308, China
[d] National Technology Innovation Center of Synthetic Biology, Tianjin, 300308, China
[e] University of Chinese Academy of Sciences, Beijing, 100049, China
[f] School of Biology and Biological Engineering, South China University of Technology, Guangzhou, 510006, China

ARTICLE INFO

Keywords:
Methanol dehydrogenase
Formaldehyde biosensor
Directed evolution
C1 bioconversion
Methanol oxidation
Methylotrophy

ABSTRACT

Methanol is a promising one-carbon feedstock for biomanufacturing, which can be sustainably produced from carbon dioxide and natural gas. However, the efficiency of methanol bioconversion is limited by the poor catalytic properties of nicotinamide adenine dinucleotide (NAD^+)-dependent methanol dehydrogenase (Mdh) that oxidizes methanol to formaldehyde. Herein, the neutrophilic and mesophilic NAD^+-dependent Mdh from *Bacillus stearothermophilus* DSM 2334 (Mdh_{Bs}) was subjected to directed evolution for enhancing the catalytic activity. The combination of formaldehyde biosensor and Nash assay allowed high-throughput and accurate measurement of formaldehyde and facilitated efficient selection of desired variants. Mdh_{Bs} variants with up to 6.5-fold higher K_{cat}/K_M value for methanol were screened from random mutation libraries. The T153 residue that is spatially proximal to the substrate binding pocket has significant influence on enzyme activity. The beneficial T153P mutation changes the interaction network of this residue and breaks the α-helix important for substrate binding into two short α-helices. Reconstructing the interaction network of T153 with surrounding residues may represent a promising strategy to further improve Mdh_{Bs}, and this study provides an efficient strategy for directed evolution of Mdh.

1. Introduction

Shortages of natural resources and grain caused by the ever-increasing world population and rapid industrial development have stimulated the search for alternative feedstocks, so as to change the current mode of biomanufacturing depending on sugar-containing feedstocks [1]. In the search for alternative feedstocks for the bio-based economy, methanol that can be produced from natural gas, carbon dioxide, and other renewable resources is emerging as a promising candidate [2]. The initial step in methanol bioconversion is the oxidation of methanol to formaldehyde, which is catalyzed by methanol dehydrogenase (Mdh) and is considered as a key rate-limiting step [3,4]. Therefore, it is of great interest to improve the catalytic activity of Mdh.

Depending on the terminal electron acceptors, Mdh is categorized into three types: nicotinamide adenine dinucleotide (NAD^+)-dependent Mdhs, PQQ (pyrroloquinoline quinone)-dependent Mdhs, and O_2-

Peer review under responsibility of KeAi Communications Co., Ltd.
* Corresponding author. Key Laboratory of Engineering Biology for Low-carbon Manufacturing, Tianjin Institute of Industrial Biotechnology, Chinese Academy of Sciences, Tianjin, 300308, China.
** Corresponding author.
E-mail addresses: wangdp@tust.edu.cn (D. Wang), wang_y@tib.cas.cn (Y. Wang).
[1] These two authors contributed equally to this work.

https://doi.org/10.1016/j.synbio.2023.05.004
Received 20 March 2023; Received in revised form 1 May 2023; Accepted 21 May 2023
Available online 8 June 2023

dependent alcohol oxidases (Aox) [5]. NAD^+-dependent Mdhs can adapt to both aerobic and anaerobic conditions, and the reducing equivalent NADH is one of the most important cofactors driving biosynthesis [6]. Therefore, NAD^+-dependent Mdhs are widely used in engineering of methanol utilization strains, such as *Escherichia coli* [7–9], *Corynebacterium glutamicum* [10–12], *Bacillus subtilis* [13], and *Saccharomyces cerevisiae* [14]. To our knowledge, multiple NAD^+-dependent Mdhs have been reported, among which four with relatively high activity from *Bacillus methanolicus* (Mdh_{Bm}) [15,16], *Cupriavidus necator* (Mdh_{Cn}) [17], *Bacillus stearothermophilus* (Mdh_{Bs}) [18], and *Lysinibacillus xylanilyticus* (Mdh_{Lx}) [19] have been purified and characterized. Almost all methanol dehydrogenases have high activity at alkaline pH (9–10) or high temperatures (45–55 °C). Mdh_{Lx}, Mdh_{Bm}, and Mdh_{Cn} all function better in buffers with a pH of 9.5, and their activities in neutral conditions are only about 10% of those in alkaline conditions. Moreover, Mdh_{Lx} and Mdh_{Bm} perform well at 55 °C and 45 °C [16,17,19]. By contrast, Mdh_{Bs} exhibits high activity at 37 °C, and its activity at pH 7.4 can reach about 80% of that at pH 5.5–6.0, which is the optimal condition [18,20]. Besides, Mdh_{Bs} shows a relatively high affinity to methanol (K_M value of 26 mM for methanol) [21]. These characteristics of Mdh_{Bs} are conducive to the synthetic methylotrophy in platform strains [22].

However, low catalytic activity is a common problem in NAD^+-dependent Mdhs. Besides, the formaldehyde reduction activity of NAD^+-dependent Mdh is much higher than the methanol oxidation activity, which would limit the efficiency of methanol bioconversion [5]. In recent years, rational design and directed evolution of Mdh has attracted much attention. For efficient screening of desired variants, it is necessary to develop a high-throughput detection method for enzyme activity or the product of methanol oxidation. Up to now, two detection methods for generated formaldehyde have been reported, formaldehyde biosensor [23–25] and Nash assay [17]. A formaldehyde-induced promoter P_{frm} has been discovered in *E. coli*, which is repressed by the transcriptional regulator FrmR in the absence of formaldehyde [26,27]. In the presence of formaldehyde, the inhibition of promoter P_{frm} is removed and the expression of downstream genes is activated. By combining promoter P_{frm} with *gfp* reporter gene to construct a biosensor system, formaldehyde concentration can be converted into easily detectable fluorescence signal *in vivo* [25]. Another traditional formaldehyde measurement method is called Nash assay [28,29]. The acetylacetone reagent reacts with formaldehyde in the presence of ammonium acetate, producing 3,5-diacetyl-1,4-dihydro-2,6-dimethylpyridine (DDL) with pale yellow color that can be quantified by absorbance at 412 nm to accurately reflect formaldehyde concentration [17]. Since formaldehyde can diffuse through the cell membrane, performing Nash assay does not need for cell lysis, which makes the measurement for formaldehyde produced *in vivo* simple and convenient. Mdh_{Lx}, Mdh_{Bm}, and Mdh_{Cn} have been subjected to directed evolution by using screening strategies based on formaldehyde biosensor or Nash assay, and variants with improved activities have been obtained. While the methanol affinity of Mdh_{Lx} and Mdh_{Cn} was significantly improved [17,30], the best Mdh_{Bm} variant showed 3.5-fold higher specific activity than the wild-type enzyme [31]. So far, no research related to directed evolution of Mdh_{Bs} that is neutrophilic and mesophilic has been conducted. In addition, formaldehyde biosensor can achieve high-throughput screening with the help of fluorescence detection instruments, but there are still inevitable false positives. In contrast, Nash assay has high accuracy due to the direct detection of formaldehyde, but the detection throughput is relatively low because the assay is limited to operation in 96-well plates.

In this study, we developed a screening strategy based on the combination of formaldehyde biosensor and Nash assay, which can achieve the high-throughput and accurate measurement of formaldehyde. This strategy was then applied for directed evolution of Mdh_{Bs}. Variants with improved catalytic efficiency were obtained and the underlying mechanisms were analyzed.

2. Materials and methods

2.1. Chemicals and materials

All chemicals were purchased from Sigma-Aldrich, Solarbio, Macklin or Thermo Fisher Scientific unless otherwise specified. 3,5-Diacetyl-1,4-dihydro-2,6-lutidine (DDL) was purchased from Dr. Ehrenstorfer (Augsburg, Germany). Restriction endonucleases and Phusion®High-Fidelity DNA Polymerase were purchased from New England Biolabs (Ipswich, MA, USA). The kits for PCR product purification and gel extraction were purchased from Promega (Madison, WI, USA). All materials for SDS-PAGE were purchased from Bio-Rad (Hercules, CA, USA). Additionally, all DNA techniques were carried out following the standard protocols for molecular biology.

2.2. Strains and plasmids

E. coli strains Trans1-T1 and DB3.1 (TransGen Biotech, Beijing, China) were used as cloning hosts, and *E. coli* strain BL21 (DE3) (TransGen Biotech, Beijing, China) was used for the expression of Mdh_{Bs}. Luciferase reporter assays, detection of formaldehyde generation and all evolutions were carried out using *E. coli* MG1655 (ATCC 700926). *E. coli* strains were cultivated with Luria–Bertani (LB) or M9 medium supplemented with required antibiotics. The complete strain and plasmid list used in this study is shown in Table S1, and the primer list is shown in Table S2. The recombinant vector for Mdh_{Bs} expression was constructed using pTrc99A, and the formaldehyde biosensor was constructed with pSB4K5. All vectors for protein purification were constructed with pET21a. Plasmids were constructed via recombination, which was conducted using the ClonExpress MultiS One Step Cloning Kit (Vazyme, Nanjing, China). Services of primer, gene synthesis and DNA sequencing were provided by GENEWIZ Inc. (Suzhou, China).

2.3. Construction of Mdh_{Bs} mutation libraries

The random mutation PCR fragment of Mdh_{Bs} was amplified by error-prone PCR with Mn^{2+}. The error-prone PCR was carried out for 30 thermal cycles and resulted in an average error rate of 2 nt/kb. The saturated mutation fragment of Mdh_{Bs} was amplified by PCR using primers containing degenerate codons. To reduce the false positives, the vector backbone was digested by the restriction enzyme *Dpn*I. The Mdh_{Bs} mutation libraries were constructed by recombination, and then transformed by electroporation into competent cells of *E. coli* MG1655-Biosensor strains.

2.4. The first round of screening by flow cytometry

After about 10 h of cultivation, the libraries were transferred into fresh M9 medium with 2 g/L glucose and induced by adding 5 μg/L tetracycline and 1 μM IPTG for another 6 h of cultivation. Then 500 mM methanol was added as a substrate, and the culture was incubated for another 40 min. To avoid evaporation of methanol, the 96-well plates and shake flasks were covered with a sealing membrane. For screening positive clones, the culture was diluted by 20-fold using M9 medium and subjected to FACS analysis, which was performed using a Beckman Coulter MoFlo XDP. Green fluorescence was measured using the 488 nm laser and 525 nm filter. Cells were gated based on FSC-H and SSC-H, and 10,000 events falling into this window were recorded. The positive clones in the mutation libraries, which had relatively high fluorescence signals (about the top 0.01%), were collected onto LB plates, and then cultured at 37 °C for 12 h. All the data were analyzed using Beckman

Summit v5.2 software.

2.5. The second round of screening by Nash assay

Cells grown overnight in LB medium were transferred into M9 medium supplemented with 2 g/L glucose and 0.1 mM IPTG for 8 h of cultivation. Nash reagent was prepared by dissolving 2 M ammonium acetate, 50 mM acetic acid, and 20 mM acetylacetone in M9 medium (pH 7.0). Nash assay was started by mixing 400 μL cell culture, 320 μL Nash reagent, and 80 μL 5 M methanol in 96-well plates. The mixture was incubated at 37 °C with shaking at 800 rpm. Samples were centrifuged at 4000 rpm for 10 min and then 200 μL supernatant was transferred to a fresh 96-well plate for measuring OD_{412nm}. In consideration of the difference in cell growth, the readout of Nash assay was normalized to cell density (OD_{600nm}).

2.6. Expression and purification of Mdh_{Bs}

E. coli BL21 (DE3) cells harboring pET21a-mdh_{Bs} were grown in LB medium at 37 °C until they reached an OD_{600nm} of 0.6–0.8, and Mdh_{Bs} expression was induced with 0.1 mM IPTG. The culture was transferred to 16 °C, incubated for 16 h, harvested by centrifugation at 6500 rpm and 4 °C for 10 min, and resuspended in phosphate buffer solution (PBS, pH 7.4). The cell extracts were then prepared by sonication. Enzymes were purified using His SpinTrap columns (GE Healthcare, USA), and then dialyzed with PBS buffer. The protein concentration was quantified using the Pierce BCA method. The purified proteins were analyzed by SDS-PAGE and the gel was stained with Coomassie brilliant blue staining solution.

2.7. Enzyme activity assays

Purified enzymes were used for activity assays. PBS-Nash reagent was prepared by dissolving 2 M ammonium acetate, 50 mM acetic acid, and 20 mM acetylacetone in PBS buffer (pH 7.4). The 200 μL reaction mixture included 40 μL PBS-Nash reagent (400 mM ammonium acetate, 10 mM acetic acid, and 4 mM acetylacetone), 0.5 mM NAD^+, 5 mM Mg^{2+}, 500 mM methanol, and 1 mg/mL enzyme. Formaldehyde produced by methanol oxidation reacted with PBS-Nash reagent at 37 °C, and the generated DDL was determined by measuring OD_{412nm} using Bio-Tek Eon microplate spectrophotometer. The standard curve of formaldehyde quantified by Nash assay reaction is shown in Supplementary Fig. S1. One unit (U) of Mdh activity was defined as the amount of enzyme that converted 1 μmol of methanol into formaldehyde per minute.

3. Results

3.1. Formaldehyde biosensor-based high-throughput screening strategy for Mdh evolution

The auto-regulated negative-feedback promoter is an important element to maintain steady-state levels of gene-expression under varying conditions, which can also be used to construct reporting systems for different needs [32]. In order to achieve high-throughput measurement of formaldehyde generated by methanol oxidation, we constructed a formaldehyde-responsive biosensor based on the formaldehyde-induced promoter P_{frm} in *E. coli* (Fig. 1A). FrmR is a member of the RcnR/CsoR family of metal-sensing transcriptional repressors and responds to formaldehyde [33]. In the absence of formaldehyde, FrmR binds to the

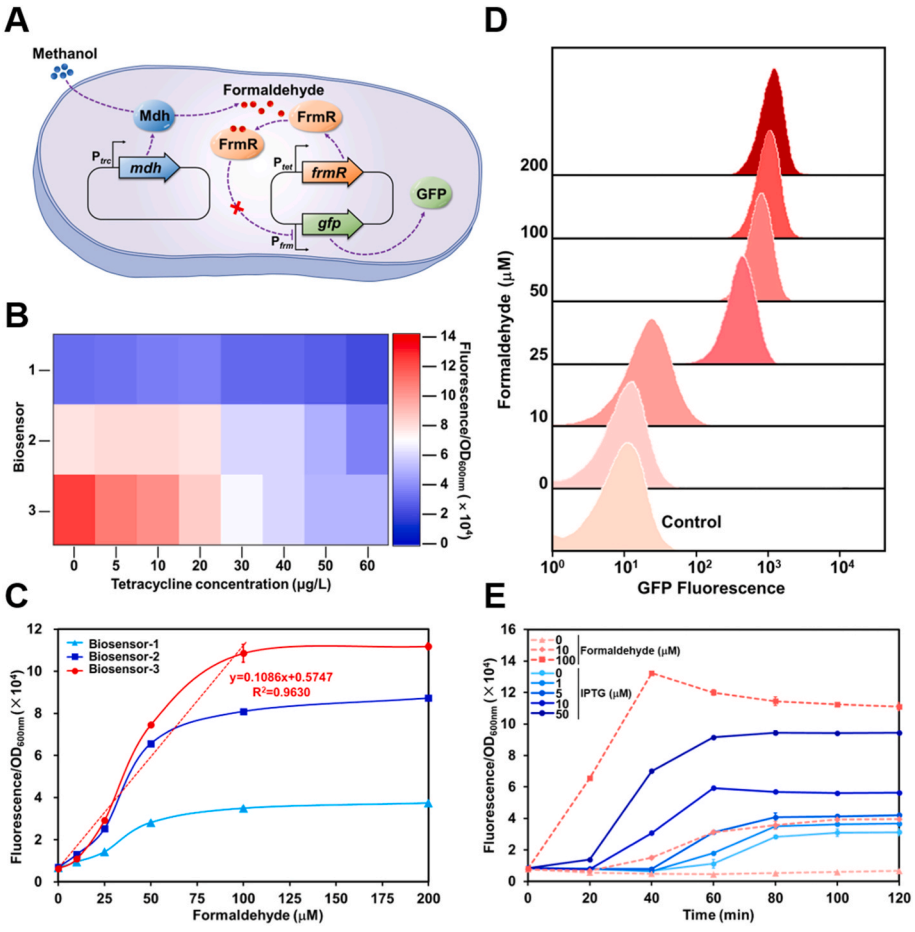

Fig. 1. Design and characterization of formaldehyde biosensor-based screening strategy. (A) Schematic diagram of the formaldehyde biosensor. Mdh, FrmR, and GFP were expressed by inducible promoters P_{trc}, P_{tet}, and P_{frm}, respectively. In the presence of formaldehyde produced by Mdh, a conformational change of FrmR was caused and the repression of P_{frm} was released, leading to GFP expression. (B) Heatmap of the induced fluorescence signals by three formaldehyde biosensors with varied concentrations of tetracycline and 100 μM formaldehyde. (C) Dose-dependent response curves of three formaldehyde biosensors. Linear fitting for Biosensor-3 (0–100 μM) is shown. Cells grown overnight in LB medium were transferred into M9 medium supplemented with 2 g/L glucose and 5 μg/L tetracycline. After 6 h of cultivation, 36 μL culture was transferred to 144 μL fresh M9 medium with 2 g/L glucose and different concentrations of formaldehyde in 96-well plates. The culture was incubated for 40 min at 37 °C with shaking at 800 rpm, and the fluorescence signals were determined. (D) Flow cytometric analysis of Biosensor-3 with different concentrations of formaldehyde. The *E. coli* MG1655 strain harboring an empty plasmid was used as the control. (E) Fluorescence signals produced by Biosensor-3 responding to formaldehyde generated by Mdh_{Bs}-catalyzed methanol oxidation. Different IPTG concentrations were used to induce Mdh_{Bs} expression. Three formaldehyde concentrations (0, 10, and 100 μM) were used as the controls. Values and error bars represent means and standard deviations (n = 3).

promoter P_{frm} region and prevents the transcription of downstream genes. In the presence of formaldehyde, the nucleophilic C36 residue of FrmR reacts with formaldehyde and causes a conformational change, resulting in the activations of downstream genes [33,34]. The formaldehyde biosensor consists of a repressor protein gene *frmR* controlled by the bidirectional tetracycline-induced promoter P_{tet} and a green fluorescent protein (GFP) gene *gfp* controlled by the formaldehyde-induced promoter P_{frm}. To optimize the operational range of the formaldehyde biosensor, we constructed three formaldehyde biosensors by using three ribosome binding sites (RBSs) selected from the Registry of Standard Biological Parts (http://parts.igem.org/) with different strengths to regulate the translation of both FrmR and GFP (Supplementary Fig. S2). Different concentrations of tetracycline (0, 5, 10, 20, 30, 40, 50, and 60 μg/L) were added to tune the transcription of FrmR. The responses to 100 μM formaldehyde for all the twenty-four combinations were then characterized (Fig. 1B). With the increase of tetracycline concentrations, the fluorescence signals generated by three formaldehyde biosensors all gradually weakened. Although higher fluorescence signals were obtained when no tetracycline was added, a better linear range of 0–100 μM was observed in the presence of 5 μg/L tetracycline for Biosensor-3 with the strong RBS (BBa_B0030, ATTAAAGAGGAGAAA) (Fig. 1C and Supplementary Fig. S3). Furthermore, the dose-response curves showed that when more than 100 μM formaldehyde was added, the fluorescence outputs were almost saturated. And when 100 μM formaldehyde was added, the induction strength of Biosensor-3 was 3.1-fold and 1.3-fold higher than those of Biosensor-1 with the weak RBS (BBa_B0031, TCACACAGGAAACC) and Biosensor-2 with the middle RBS (BBa_B0032, TCACACAGGAAAG), respectively (Fig. 1C). In addition, to test the possibility of biosensor-enabled fluorescence activated cell sorting (FACS), the fluorescence outputs of Biosensor-3 with different concentrations of formaldehyde (0, 10, 25, 50, 100, and 200 μM) under 5 μg/L tetracycline were analyzed by using flow cytometry. Without derepression of formaldehyde, the fluorescence signal produced by the biosensor was similar to that of the negative control (*E. coli* MG1655 harboring an empty pTrc99A plasmid), demonstrating a low background fluorescence signal. Dose-dependent fluorescence signals were observed with the increase in formaldehyde concentrations, suggesting that this formaldehyde biosensor can be used for high-throughput formaldehyde measurement by using flow cytometry (Fig. 1D). All the tests were carried out in the wild-type *E. coli* MG1655 strain, which possesses an endogenous formaldehyde degradation pathway. However, it seemed that the formaldehyde degradation pathway did not affect the dose-dependent response of the biosensor to formaldehyde. Therefore, this pathway was not blocked in this study.

In order to apply the formaldehyde biosensor for directed evolution of Mdh_{Bs}, the biosensor plasmid and Mdh_{Bs} expressing plasmid were co-transformed into *E. coli* MG1655. After addition of methanol, Mdh_{Bs} catalyzed the oxidation of methanol to formaldehyde, the concentration of which was translated into fluorescence signal by the biosensor. In theory, the higher activity of Mdh_{Bs} variants showed, the more formaldehyde generated *in vivo*, and the stronger fluorescence signal detected (Fig. 1A). To facilitate screening of Mdh_{Bs} variants with improved activity, the concentration of formaldehyde produced by Mdh_{Bs} should not exceed the operational range of the biosensor (approximately 10–100 μM). Therefore, we optimized the expression level of Mdh_{Bs} by adjusting the usage of isopropyl-β-D-thiogalactopyranoside (IPTG), the inducer for Mdh_{Bs} expression. A positive relationship between IPTG usage and Mdh_{Bs} expression level was observed (Supplementary Fig. S4). In the absence of IPTG, some fluorescence signals were detected 60 min after the addition of methanol, indicating a certain level of leakage expression of Mdh_{Bs}. With the same amount of methanol and increased usage of IPTG, the fluorescence signals generated by the formaldehyde biosensor gradually increased (Fig. 1E). In the presence of 5 μM IPTG, the generation curve of fluorescence signals was similar to that of the positive control of 10 μM formaldehyde. When the IPTG concentration was over 10 μM, the fluorescence signals exceeded the positive control of 10 μM formaldehyde. To ensure that only Mdh_{Bs} variants with enhanced formaldehyde formation can be screened, a low IPTG concentration of 1 μM was used to induce the expression of Mdh_{Bs} variants in the subsequent directed evolution experiments.

3.2. High-throughput screening of Mdh_{Bs} variants from random mutation libraries

To obtain Mdh_{Bs} variants with improved catalytic activities, we applied the formaldehyde biosensor-based high-throughput screening strategy for directed evolution of Mdh_{Bs}. Error-prone PCR was used to generate random mutation libraries of Mdh_{Bs} using the wild-type mdh_{Bs} gene as the template. The mutation libraries were subjected to FACS analysis with the wild-type Mdh_{Bs} as a control. With the addition of methanol, about 0.036% of cells in the mutation libraries showed increased fluorescence intensities, while the proportion of cells was only 0.003% without methanol (Fig. 2A). The 0.01% of cells with highest fluorescence intensities were isolated by using flow cytometry.

In order to further determine the efficiency of formaldehyde biosensor-based screening, we measured the fluorescence intensity and the formaldehyde produced by methanol oxidation of the 84 strains obtained from the first round of sorting in 96-well plates. Five strains showed strong background fluorescence signals in the absence of methanol, suggesting that the expression of GFP in these strains was no longer repressed by the formaldehyde responsive regulator FrmR (Fig. 2B). This was possibly due to the introduction of unexpected mutations in the regulatory sequence. In the presence of methanol, 76 strains showed significantly improved fluorescence signals compared with those of the wild-type strain (Fig. 2C), which were expected to harbor Mdh_{Bs} variants with improved catalytic activities. However, formaldehyde measurement by Nash assay showed that only 36 strains produced more formaldehyde than the wild-type control (Fig. 2D). The difference between the two assays indicated that a certain proportion of strains sorted by FACS were false positives, which could not be excluded effectively by retesting their fluorescence intensities. Therefore, a first round of screening by FACS, followed by a second round of screening by Nash assay could balance the tradeoff between throughput and accuracy of formaldehyde measurement and facilitate screening of Mdh_{Bs} variants (Fig. 3A).

After the initial test, total 3455 strains obtained by the first round of FACS entered the second round of screening for determining their formaldehyde formation rates by Nash assay. Compared with the formaldehyde formation of the control strain harboring wild-type Mdh_{Bs}, 2062 strains showed higher formaldehyde formation, accounting for about 60% of all the tested strains (Fig. 3B). The highest 15% of strains with at least one-fold increase in formaldehyde formation were subjected to Mdh_{Bs} plasmid sequencing. The results revealed 32 kinds of variants, of which 18 had amino acid substitutions. The rest 14 variants had no missense mutations in Mdh_{Bs} but several synonymous mutations or promoter and RBS mutations. These mutations may have an influence on the expression level of Mdh_{Bs}.

3.3. Directed evolution of Mdh_{Bs} targeting the substrate binding pocket

In addition to Mdh_{Bs} random mutation libraries, we also constructed and screened a Mdh_{Bs} mutation library targeting the substrate binding pocket. It has been reported that iso-propanol is the most favorable substrate for Mdh_{Bs} and the substrate binding pocket may not be ideal for methanol [35]. According to the crystal structure Mdh_{Bs} (PDB: 6IQD) and sequence alignment with the dehydrogenases from *Geobacillus stearothermophilus* LLD-R (PDB: 1RJW), *Pseudomonas aeruginosa* (PDB: 1LLU), and *E. coli* K-12 (PDB: 4GKV), the conserved residues C38, T40, H61, and C148 are suggested to be the key residues for substrate binding [35]. Therefore, a combinatorial site-saturated mutation library for these four residues were constructed. The library was subjected to screening using formaldehyde biosensor-based FACS and Nash assay.

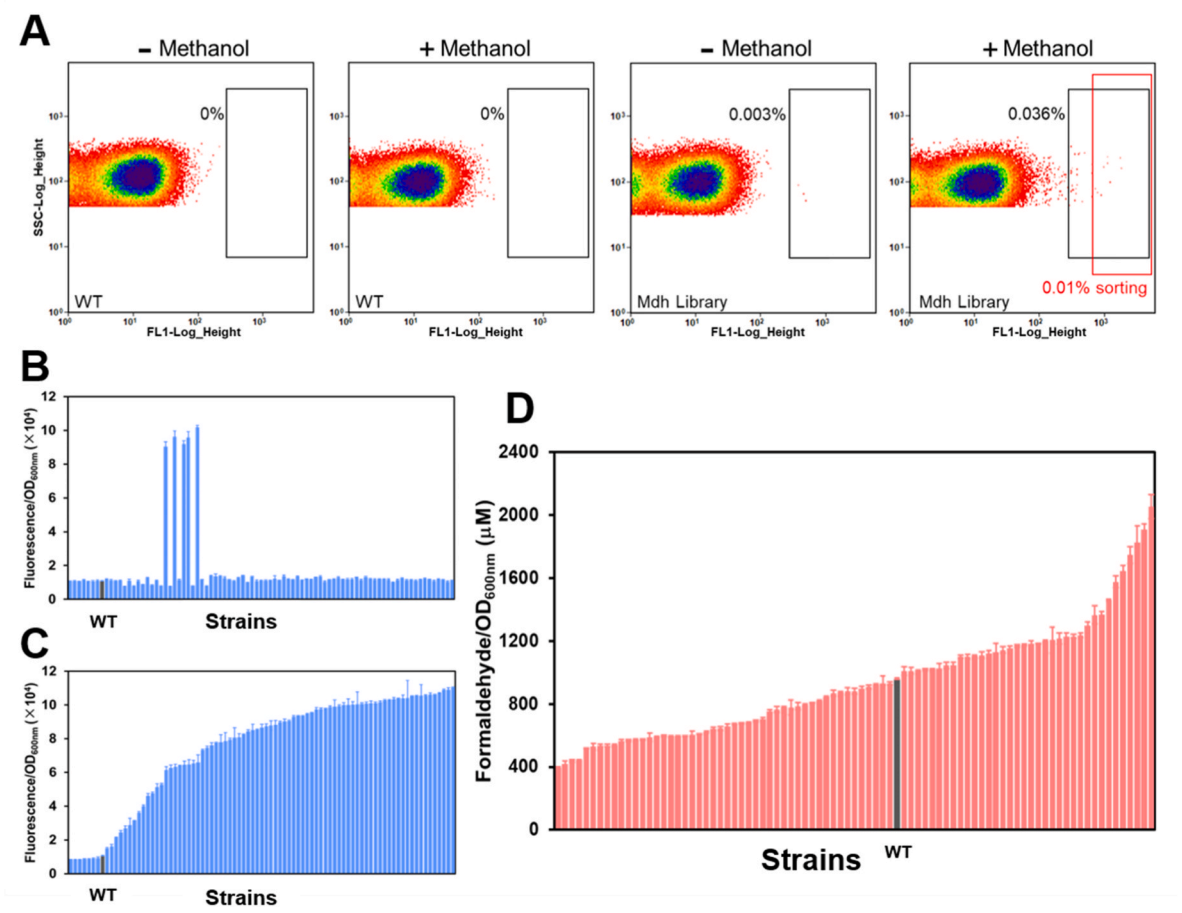

Fig. 2. Preliminary screening tests for random mutant libraries. (A) Flow cytometric analysis for cells harboring the wild-type Mdh_{Bs} and random mutation libraries without or with methanol. The black frame represents the same gate in the four analyses. (B) The fluorescence intensities of the 84 sorted strains in the absence of methanol. (C) The fluorescence intensities of the 84 sorted strains in the presence of methanol. (D) The formaldehyde produced by methanol oxidation of the 84 sorted strains.

Unfortunately, no variants with significantly improved catalytic activities were obtained, suggesting directly modifying the substrate binding pocket cannot optimize the methanol binding and oxidative reaction.

3.4. Enzyme activity assay of the screened Mdh_{Bs} variants

In order to confirm the function of missense mutations and exclude the potential effects of other undetected mutations on the plasmid backbone or the chromosome introduced during library construction and screening, we reconstructed the expression plasmids for the 18 variants. After reconstruction, six variants, $Mdh_{Bs}^{I51V + V319A}$, Mdh_{Bs}^{V79A}, $Mdh_{Bs}^{N214D + E309K}$, $Mdh_{Bs}^{K242E + D339G}$, Mdh_{Bs}^{E33K}, and $Mdh_{Bs}^{K72T + T153P}$, showed 32%–193% increase in formaldehyde formation in whole-cell bioconversion compared with the wild-type Mdh_{Bs} (Fig. 4A). The remaining 12 variants showed similar activities with the wild-type Mdh_{Bs}. The different methanol oxidation activities before and after the reconstruction of Mdh_{Bs} expression plasmids may be due to the unidentified mutations on the plasmid backbone or the chromosome of the host introduced during library construction and screening.

To characterize the enzyme activities of the six reconstructed Mdh_{Bs} variants, they were heterologously expressed using the pET21a vector in *E. coli* BL21 (DE3) strain. A *C*-terminal His tag was fused to Mdh_{Bs} variants. SDS-PAGE analysis showed that all the six Mdh_{Bs} variants and the wild-type enzyme were successfully overexpressed (Supplementary Fig. S5A). However, part of expressed $Mdh_{Bs}^{N214D + E309K}$, $Mdh_{Bs}^{K242E + D339G}$, and $Mdh_{Bs}^{K72T + T153P}$ proteins were inclusion bodies, especially $Mdh_{Bs}^{N214D + E309K}$, resulting in reduced expression of soluble proteins (SupplementaryFigs. S5B and S5C). The target enzymes were purified using a His SpinTrap column and were analyzed by SDS-PAGE (Fig. 4B). Then the activities of the purified enzymes were measured to identify the best candidate. Among the six variants tested, the activities of $Mdh_{Bs}^{I51V + V319A}$, $Mdh_{Bs}^{K242E + D339G}$, and Mdh_{Bs}^{E33K} were lower than or similar to that of the wild-type Mdh_{Bs} (Fig. 4C). The observed higher formaldehyde formation rates in whole-cell bioconversion were possibly due to the potential effects of these mutations on soluble expression or the different test conditions *in vivo* and *in vitro*. The specific activities of the rest three variants $Mdh_{Bs}^{K72T + T153P}$, $Mdh_{Bs}^{N214D + E309K}$ and Mdh_{Bs}^{V79A} were 28.8 mU/mg, 23.8 mU/mg, and 14.2 mU/mg, approximately 2.5-fold, 2.1-fold, and 1.2-fold higher than the wild-type enzyme, respectively (Fig. 4C). The improvement of $Mdh_{Bs}^{N214D + E309K}$ in specific activity (110%) was much higher than that in whole-cell bioconversion (38%), which should be due to its poorly soluble expression *in vivo* (Supplementary Figs. S5B and S5C). We also tested the activity of Mdh_{Cn}^{CT4-1} variant at 37 °C, pH 7.4, which has been reported from *Cupriavidus necator* [17]. The result showed that the specific activity of Mdh_{Cn}^{CT4-1} variant was 14.9 mU/mg, which was less than 5% of the optimal activity under alkaline conditions and almost half of the activity of $Mdh_{Bs}^{K72T + T153P}$ variant (Fig. 4D and Supplementary Fig. S6).

Kinetic parameters for the best two variants were determined. The K_M values of $Mdh_{Bs}^{K72T + T153P}$ and $Mdh_{Bs}^{N214D + E309K}$ variants were 9.84 mM and 18.19 mM, which were decreased by 67% and 39% compared with the wild-type enzyme (30.03 mM) (Table 1). To unify the enzyme activity assay method for the whole-cell catalysts and purified enzymes, Nash assay capable of quantifying the generated formaldehyde by

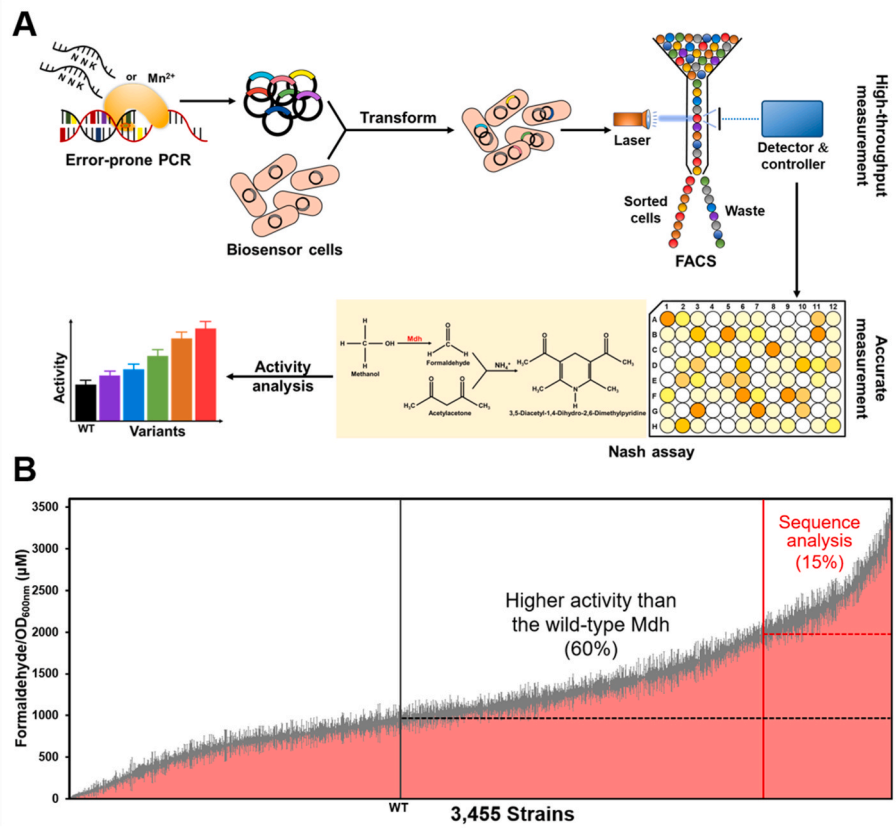

Fig. 3. High-throughput and accurate screening strategy for Mdh evolution. (A) Schematic diagram of high-throughput and accurate screening process. (B) The formaldehyde measurement by Nash assay for the 3455 strains obtained by the first round of FACS. Values and error bars represent means and standard deviations (n = 3).

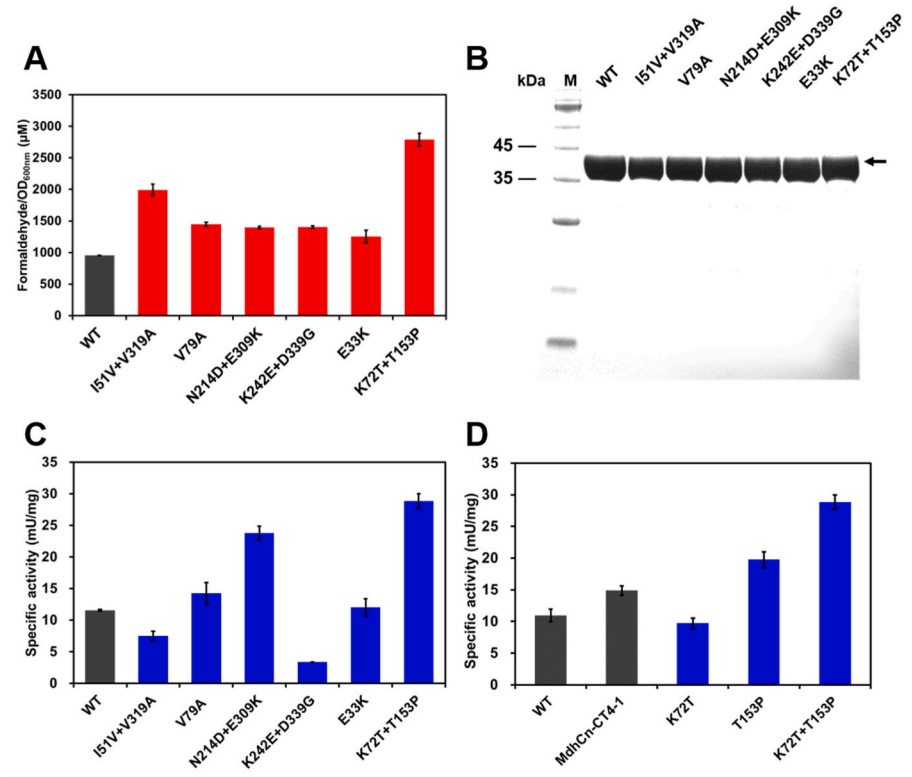

Fig. 4. Activity assay of the wild-type Mdh_{Bs} and six reconstructed variants. (A) The whole-cell formaldehyde formation of the wild-type Mdh_{Bs} and six reconstructed variants measured by Nash assay. Except for $Mdh_{Bs}^{I51V\ +\ V319A}$, the other five variants all contain synonymous mutations. Mdh_{Bs}^{V79A} contains C106C (C318T), $Mdh_{Bs}^{N214D\ +\ E309K}$ and $Mdh_{Bs}^{K242E\ +\ D339G}$ contain E8E (A24G), Mdh_{Bs}^{E33K} contains V70V (C210T), and $Mdh_{Bs}^{K72T\ +\ T153P}$ contains R163R (G489A), S236S (T708C), and K241K (A723G). (B) SDS-PAGE analysis of the purified enzymes for the wild-type Mdh_{Bs}, $Mdh_{Bs}^{I51V\ +\ V319A}$, Mdh_{Bs}^{V79A}, $Mdh_{Bs}^{N214D\ +\ E309K}$, $Mdh_{Bs}^{K242E\ +\ D339G}$, Mdh_{Bs}^{E33K}, and $Mdh_{Bs}^{K72T\ +\ T153P}$ variants. (C) The specific enzyme activity of the wild-type Mdh_{Bs} and six reconstructed variants. (D) The specific enzyme activity of the wild-type Mdh_{Bs}, Mdh_{Bs}^{K72T}, Mdh_{Bs}^{T153P}, $Mdh_{Bs}^{K72T\ +\ T153P}$ and Mdh_{Cn}^{CT4-1} variants. Values and error bars represent means and standard deviations (n = 3).

Table 1
Kinetic parameters of the wild-type Mdh_{Bs}, $Mdh_{Bs}^{N214D + E309K}$, and $Mdh_{Bs}^{K72T + T153P}$ variants[a].

Enzyme	V_{max} (mU/mg)	K_M (mM)	K_{cat} (s^{-1})	K_{cat}/K_M ($M^{-1}\cdot s^{-1}$)
Wild-type	11.54 ± 0.15	30.03 ± 4.63	0.007 ± 0.001	0.233
$Mdh_{Bs}^{N214D + E309K}$	23.81 ± 1.08	18.19 ± 3.27	0.013 ± 0.001	0.715
$Mdh_{Bs}^{K72T + T153P}$	28.84 ± 1.16	9.84 ± 0.67	0.015 ± 0.001	1.524

[a] Enzyme activities were determined by using the Nash assay method with methanol as a substrate at 37 °C, pH 7.4. The values were calculated based on Michaelis-Menten fit and the data sets shown indicate mean ± standard deviation (n = 3).

methanol oxidation was used to determine the kinetic parameters. The K_M value of the wild-type Mdh_{Bs} determined by using the Nash assay (30.03 mM) is comparable to that determined by the NADH measurement (26 mM) [21], suggesting the usability of the Nash assay in kinetic measurement. The catalytic efficiencies (K_{cat}/K_M values) of $Mdh_{Bs}^{K72T + T153P}$ and $Mdh_{Bs}^{N214D + E309K}$ were 1.524 M^{-1} s^{-1} and 0.715 M^{-1} s^{-1}, which were 6.5-fold and 3.1-fold higher than that of the wild-type enzyme, respectively. Since $Mdh_{Bs}^{K72T + T153P}$ variant represented the best performance both *in vivo* and *in vitro*, it was selected for the further investigation.

3.5. Characterization of the functions of K72T and T153P mutations

Besides the two missense mutations (K72T and T153P), $Mdh_{Bs}^{K72T + T153P}$ contains another three synonymous mutations of R163R (G489A), S236S (T708C), and K241K (A723G). We first removed the three synonymous mutations from the gene sequence and constructed three variants containing single or double mutations of K72T and T153P. Expression test showed that genes without the three synonymous mutations were all poorly expressed (Supplementary Fig. S7A). These results indicated that although K72T and T153P mutations improved the catalytic activity of Mdh_{Bs}, they decreased the protein expression level.

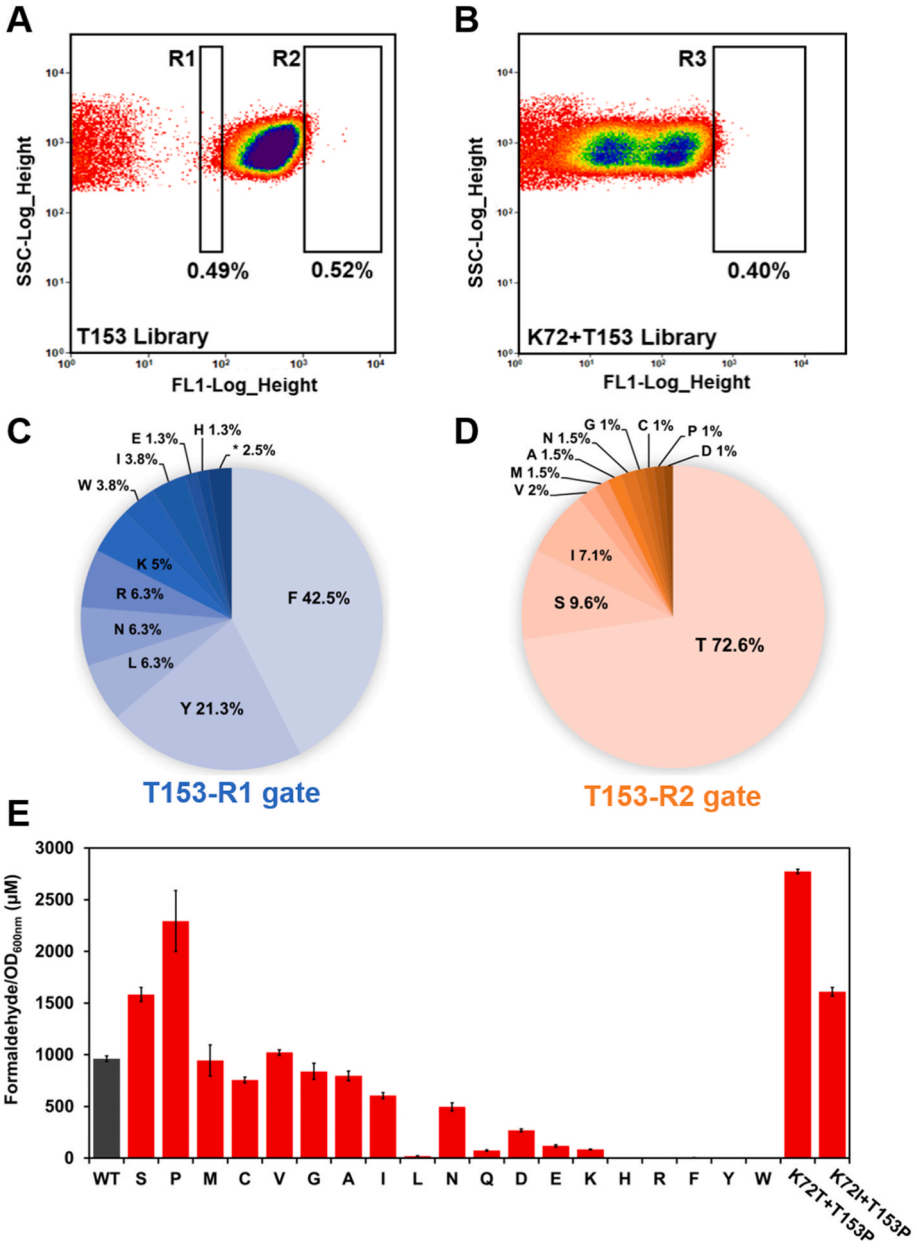

Fig. 5. Characterization of the functions of K72T and T153P mutations. (A) Flow cytometric analysis of the T153 saturated mutation library. (B) Flow cytometric analysis of the K72 and T153 double-saturated mutation library. (C) Distribution of mutation types analyzed from gene sequencing of cells from the T153-R1 gate. (D) Distribution of mutation types analyzed from gene sequencing of cells from the T153-R2 gate. (E) The whole-cell formaldehyde formation of the T153 variants measured by Nash assay. Values and error bars represent means and standard deviations (n = 3).

Considering easy purification of recombinant proteins, subsequent experiments were conducted on the basis of Mdh_{Bs}^{RSK} retaining the three synonymous mutations. Variants containing single mutation of K72T or T153P were heterologously expressed and purified (Supplementary Fig. S7B). Purified enzymes were tested for activities *in vitro* to explore the contributions of K72T and T153P to the catalytic activities. The specific activities of Mdh_{Bs}^{K72T} and Mdh_{Bs}^{T153P} were 9.7 mU/mg and 19.8 mU/mg, respectively. While the K72T mutation showed no significant effects on enzyme activity, the T153P mutation resulted in a 1.8-fold increase in the enzyme activity compared with the wild-type enzyme (Fig. 4D). It is suggested that T153P is a key mutation in enhancing the catalytic activity of Mdh_{Bs}. In addition, it is worth noting that the activity of $Mdh_{Bs}^{K72T + T153P}$ was 1.5-fold higher than that of Mdh_{Bs}^{T153P}. This suggests that although the K72T mutation does not function alone, K72T and T153P mutations have synergistic effects on enzyme activity.

In order to further explore the effects of T153 residue on Mdh_{Bs} activity and obtain Mdh_{Bs} variants with higher activities, a T153 saturated mutation library was constructed and analyzed by flow cytometry based on the formaldehyde biosensor. Cells with high fluorescence signals (0.52%, R2 gate) and low fluorescence signals (0.49%, R1 gate) were selected for sorting (Fig. 5A). Cells sorted from the library were sequenced for *mdh*$_{Bs}$ gene, and certain mutation patterns were found. For cells with low fluorescence signals, T153F and T153Y accounted for 42.5% and 21.3% of the total detected mutations, respectively (Fig. 5C). Another aromatic amino acid mutation T153W was also enriched (3.8%). It seems that mutation of threonine to aromatic amino acids would impair the enzyme activity. For cells with high fluorescence signals, approximately 72.6% of cells harbor Mdh_{Bs} with unchanged amino acid sequence but some have synonymous T153T mutations (Fig. 5D). T153S and T153I accounted for 9.6% and 7.1% of detected mutations. And the remaining 10.7% was composed of different amounts of T153V, T153 M, T153A, T153 N, T153G, T153C, T153P, and T153D mutations. Next, we constructed all the 19 Mdh_{Bs} variants with T153 mutations and determined their formaldehyde formation activities in whole-cell bioconversion. All the variants were successfully expressed and their expression levels were not significantly changed (Supplementary Fig. S8). Mdh_{Bs}^{T153P} was still the best variant and Mdh_{Bs}^{T153S} also showed improved activity compared with the wild-type enzyme (Fig. 5E). The mutations enriched in the cells with high fluorescence signals, such as T153V, T153 M, T153A, T153G, T153C, did not impaired the enzyme activity. However, three aromatic amino acid mutations (T153F, T153Y, and T153W) enriched in the cells with low fluorescence signals, together with T153L, T153R, and T153H mutations almost completely deactivated the enzyme. Since single site mutation of T153 did not produce variants better than $Mdh_{Bs}^{K72T + T153P}$, we constructed a K72 and T153 double-saturated mutation library and analyzed it by FACS. The 0.40% of cells with highest fluorescence signals (R3 gate) were sorted and tested for the formaldehyde formation rates (Fig. 5B). Besides $Mdh_{Bs}^{K72T + T153P}$, only the $Mdh_{Bs}^{K72I + T153P}$ variant showed higher activities than the wild-type enzyme but it still did not outperform $Mdh_{Bs}^{K72T + T153P}$ (Fig. 5E).

3.6. Structural analysis of the T153 variants

The best variant $Mdh_{Bs}^{K72T + T153P}$ obtained in this study had a 67% decrease in K_M for methanol and 6.5-fold higher catalytic efficiency than the wild-type enzyme. Based on the crystal structure [35], the T153 residue is spatially proximal to the substrate binding pocket and locates in the same α-helix with C148, a key residue for methanol binding. Saturated mutation of T153 suggests that this residue has significant influence on enzyme activity. While T153S and T153P enhanced enzyme activity, mutation of threonine to aromatic amino acids completely deactivated Mdh_{Bs}. The structures of the wild-type Mdh_{Bs} and three variants Mdh_{Bs}^{T153S}, Mdh_{Bs}^{T153P}, and Mdh_{Bs}^{T153F} were predicted by using Alphafold2 [36] and the interactions of the residue at 153 position with surrounding residues were analyzed. Interestingly, while T153S and T153F did not affect the structure of this α-helix, T153P broke the structure into two short α-helices combined with a short loop (Fig. 6). The interaction network of T153 was also largely affected by amino acid substitutions. In the original structure, T153 formed hydrogen bonds with A149, G150, A156, and L157. For Mdh_{Bs}^{T153P} variant, only the hydrogen bonds with A156 and L157 were maintained and the rest were disrupted. Moreover, substitution of threonine with phenylalanine resulted in the formation of the C–H … π interaction with L157, which

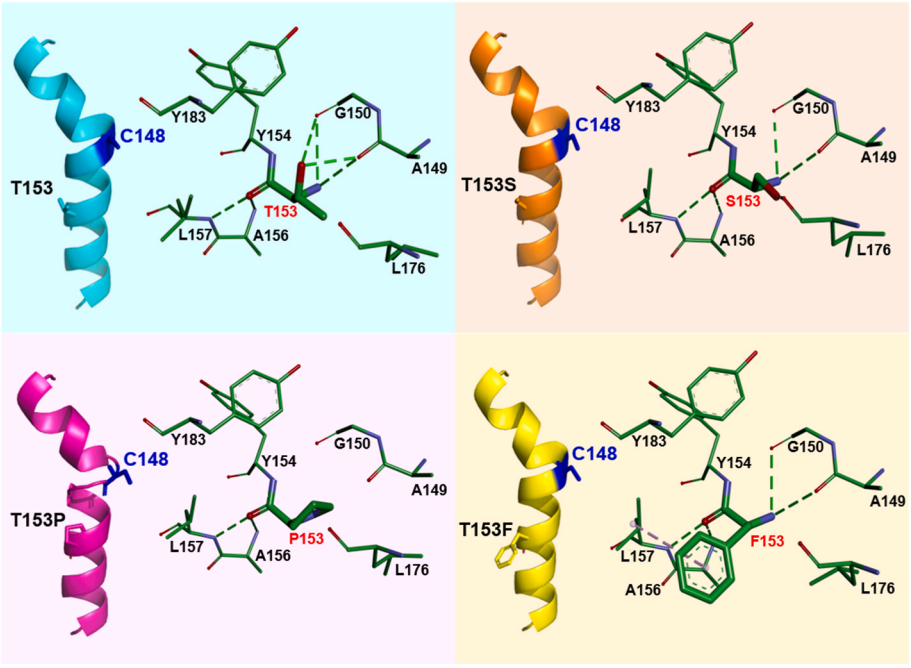

Fig. 6. Structures and interaction networks of the wild-type Mdh_{Bs}, Mdh_{Bs}^{T153S}, Mdh_{Bs}^{T153P}, and Mdh_{Bs}^{T153F} variants. Structures were predicted by Alphafold2 [36] and the interaction networks at the 153 residue were analyzed by using PyMOL.

may account for the loss of Mdh activity after substitution of aromatic amino acids. Therefore, reconstructing the interaction network of T153 with surrounding residues may represent a promising strategy to further improve Mdh_{Bs}.

4. Discussion

Methanol oxidation is a rate-limiting step of C1 bioconversion, and Mdh is the key enzyme for the process [5,37,38]. Screening and engineering enzymes to improve the catalytic activity and substrate affinity of Mdhs has recently attracted great attention. However, compared with other enzymes involved in methylotrophy such as 3-hexulose-6-phosphate synthase (Hps) and 6-phospho-3-hexuloisomerase (Phi) with high activities, the activities of screened and engineered Mdhs are still unsatisfactory [17,30,31]. In this study, we developed a screening strategy for directed evolution of Mdh based on high-throughput and accurate measurement of formaldehyde, which was enabled by an optimized formaldehyde biosensor and Nash color reaction, respectively. Compared with previous studies by using formaldehyde biosensor for directed evolution of Mdh [30], the integration of Nash assay enabled more accurate measurement of formaldehyde and served as a complementary method for the second round of screening after the first round of screening using the formaldehyde biosensor. By coupling the phage reproduction with the formaldehyde generation by using the formaldehyde biosensor, phage-assisted noncontinuous evolution (PANCE) has been successfully applied for directed evolution of Mdh [31]. However, the operation of PANCE required a set of sophisticated evolution devices. In contrast, the two-round screening strategy with formaldehyde biosensor and Nash assay used in this study was simple to operate and was successfully used for the directed evolution of the neutrophilic and mesophilic Mdh_{Bs}, producing variants with up to 6.5-fold higher catalytic efficiency.

Biosensor-based FACS has been widely used in high-throughput screening of enzyme variants, but false positives are usually difficult to eliminate [39–41]. In this study, there were two main types of false positives during screening: individuals with enhanced background fluorescence signals even without addition of the substrate methanol and individuals with enhanced fluorescence signals after methanol addition but unchanged Mdh_{Bs} activities. We found that the first type of false positives was rare and most cells sorted by FACS showed significantly enhanced fluorescence signals with methanol addition compared with the wild-type control. However, only approximately 60% of cells sorted by FACS showed improved formaldehyde formation rates, suggesting that the second type of false positives were dominant. Such false positives may be the result of a variety of factors, such as random mutations in the chromosome, the plasmid, the biosensor construct, or the regulatory elements for Mdh_{Bs}. Therefore, it is necessary to reconstruct the variants and accurately measure the formaldehyde production by using Nash assay. Furthermore, some variants we obtained contained only synonymous mutations. They were selected after two rounds of screening because of the increased intracellular catalytic activity caused by the elevated expression levels of Mdh_{Bs}. Such cases are difficult to avoid in screening of random mutation libraries. By using the high-throughput screening strategy combining the formaldehyde biosensor and Nash assay, false positives can be excluded and desired variants can be selected.

CRediT authorship contribution statement

Jin Qian: Methodology, Investigation, Validation, Data curation, Writing – original draft, Writing – review & editing, Visualization. **Liwen Fan:** Methodology, Investigation, Data curation, Formal analysis, Visualization. **Jinxing Yang:** Methodology, Investigation, Software, Visualization. **Jinhui Feng:** Formal analysis, Software. **Ning Gao:** Methodology, Investigation. **Guimin Cheng:** Methodology, Investigation. **Wei Pu:** Methodology, Investigation. **Wenjuan Zhou:** Data curation, Formal analysis. **Tao Cai:** Formal analysis, Software. **Shuang Li:** Supervision, Resources. **Ping Zheng:** Conceptualization, Methodology, Data curation, Formal analysis, Supervision, Resources, Funding acquisition, Project administration. **Jibin Sun:** Supervision, Resources, Funding acquisition. **Depei Wang:** Supervision, Resources, Funding acquisition. **Yu Wang:** Conceptualization, Methodology, Investigation, Validation, Data curation, Formal analysis, Writing – original draft, Writing – review & editing, Visualization, Supervision, Funding acquisition, Project administration, All authors have read and agreed to the final manuscript.

Declaration of competing interest

Tianjin Institute of Industrial Biotechnology has filed a patent application. The authors declare no competing financial or non-financial interests.

Acknowledgements

This research was supported by the grants from the National Key Research and Development Program of China (2018YFA0901500), the National Natural Science Foundation of China (32070083 and 32222004), the Youth Innovation Promotion Association of Chinese Academy of Sciences (2021177), the Tianjin Synthetic Biotechnology Innovation Capacity Improvement Project (TSBICIP-KJGG-008), and the Innovation Fund of Haihe Laboratory of Synthetic Biology. We thank Ms. Lixian Wang and Ms. Jie Zhang of Tianjin Institute of Industrial Biotechnology for the help with FACS analysis and protein purification.

Appendix A. Supplementary data

Supplementary data to this article can be found online at https://doi.org/10.1016/j.synbio.2023.05.004.

References

[1] Clomburg JM, Crumbley AM, Gonzalez R. Industrial biomanufacturing: the future of chemical production. Science 2017;355(6320):38. https://doi.org/10.1126/science.aag0804.
[2] Wang Y, Fan LW, Tuyishime P, Zheng P, Sun JB. Synthetic methylotrophy: a practical solution for methanol-based biomanufacturing. Trends Biotechnol 2020;38(6):650–66. https://doi.org/10.1016/j.tibtech.2019.12.013.
[3] Cai T, Sun HB, Qiao J, Zhu LL, Zhang F, Zhang J, et al. Cell-free chemoenzymatic starch synthesis from carbon dioxide. Science 2021;373(6562):1523–7. https://doi.org/10.1126/science.abh4049.
[4] Wu S, Bornscheuer UT. A chemoenzymatic cascade with the potential to feed the world and allow humans to live in space. Eng Microbiol 2022;2(1):10006–8. https://doi.org/10.1016/j.engmic.2021.100006.
[5] Le TK, Lee YJ, Han GH, Yeom SJ. Methanol dehydrogenases as a key biocatalysts for synthetic methylotrophy. Front Bioeng Biotechnol 2021;9:787791. https://doi.org/10.3389/fbioe.2021.787791.
[6] Whitaker WB, Sandoval NR, Bennett RK, Fast AG, Papoutsakis ET. Synthetic methylotrophy: engineering the production of biofuels and chemicals based on the biology of aerobic methanol utilization. Curr Opin Biotechnol 2015;33:165–75. https://doi.org/10.1016/j.copbio.2015.01.007.
[7] Chen FY, Jung HW, Tsuei CY, Liao JC. Converting *Escherichia coli* to a synthetic methylotroph growing solely on methanol. Cell 2020;182(4):933–46. https://doi.org/10.1016/j.cell.2020.07.010.
[8] Chuang W, Jie R, Libang Z, Zhidong L, Lin C, An Z. An aldolase-catalyzed new metabolic pathway for the assimilation of formaldehyde and methanol to synthesize 2-keto-4-hydroxybutyrate and 1,3-propanediol in *Escherichia coli*. ACS Synth Biol 2019;8(11):2483–93. https://doi.org/10.1021/acssynbio.9b00102.
[9] He H, Edlich MC, Lindner SN, Bar EA. Ribulose monophosphate shunt provides nearly all biomass and energy required for growth of *E. coli*. ACS Synth Biol 2018;7(6):1601–11. https://doi.org/10.1021/acssynbio.8b00093.
[10] Tuyishime P, Wang Y, Fan L, Zhang Q, Li Q, Zheng P, et al. Engineering *Corynebacterium glutamicum* for methanol-dependent growth and glutamate production. Metab Eng 2018;49:220–31. https://doi.org/10.1016/j.ymben.2018.07.011.
[11] Wang Y, Fan LW, Tuyishime P, Liu J, Zhang K, Gao N, et al. Adaptive laboratory evolution enhances methanol tolerance and conversion in engineered *Corynebacterium glutamicum*. Commun Biol 2020;3(1):217. https://doi.org/10.1038/s42003-020-0954-9.
[12] Hennig G, Haupka C, Brito LF, Ruckert C, Cahoreau E, Heux S, et al. Methanol-essential growth of *Corynebacterium glutamicum*: adaptive laboratory evolution

overcomes limitation due to methanethiol assimilation pathway. Int J Mol Sci 2020;21(10):3617. https://doi.org/10.3390/ijms21103617.
[13] Bo G, Ning Z, Jieying D, Yang G, Shiru J, Ying H, et al. Constructing a methanol-dependent *Bacillus subtilis* by engineering the methanol metabolism. J Biotechnol 2022;343:128–37. https://doi.org/10.1016/j.jbiotec.2021.12.005.
[14] Dai Z, Gu H, Zhang S, Xin F, Zhang W, Dong W, et al. Metabolic construction strategies for direct methanol utilization in *Saccharomyces cerevisiae*. Bioresour Technol 2017;245:1407–12. https://doi.org/10.1016/j.biortech.2017.05.100.
[15] Devries GE, Arfman N, Terpstra P, Dijkhuizen L. Cloning, expression, and sequence-analysis of the *Bacillus methanolicus* C1 methanol dehydrogenase gene. J Bacteriol 1992;174(16):5346–53. https://doi.org/10.1128/JB.174.16.5346-5353.1992.
[16] Krog A, Heggeset TM, Müller JE, Kupper CE, Schneider O, Vorholt JA, et al. Methylotrophic *Bacillus methanolicus* encodes two chromosomal and one plasmid born NAD^+ dependent methanol dehydrogenase paralogs with different catalytic and biochemical properties. PLoS One 2013;8(3):e59188. https://doi.org/10.1371/journal.pone.0059188.
[17] Wu TY, Chen CT, Liu JT, Bogorad IW, Damoiseaux R, Liao JC. Characterization and evolution of an activator-independent methanol dehydrogenase from *Cupriavidus necator* N-1. Appl Microbiol Biotechnol 2016;100(11):4969–83. https://doi.org/10.1007/s00253-016-7320-3.
[18] Marian CS, Christopher JB, Barbara CAD, David JM. A new alcohol dehydrogenase, reactive towards methanol, from *Bacillus stearothermophilus*. Biochem J 1988;252:661–6. https://doi.org/10.1042/bj2520661.
[19] Lee JY, Park SH, Oh SH, Lee JJ, Kwon KK, Kim SJ, et al. Discovery and biochemical characterization of a methanol dehydrogenase from *Lysinibacillus xylanilyticus*. Front Bioeng Biotechnol 2020;8:67. https://doi.org/10.3389/fbioe.2020.00067.
[20] Israel E, Nathan G. Prototrophic thermophilic *Bacillus*: isolation, properties, and kinetics of growth. J Bacteriol 1969;99(2):414–7. https://doi.org/10.1128/jb.99.2.414-417.1969.
[21] Fan L, Wang Y, Tuyishime P, Gao N, Li Q, Zheng P, et al. Engineering artificial fusion proteins for enhanced methanol bioconversion. Chembiochem 2018;19(23):2465–71. https://doi.org/10.1002/cbic.201800424.
[22] Whitaker WB, Jones JA, Bennett RK, Gonzalez JE, Vernacchio VR, Collins SM, et al. Engineering the biological conversion of methanol to specialty chemicals in *Escherichia coli*. Metab Eng 2017;39:49–59. https://doi.org/10.1016/j.ymben.2016.10.015.
[23] Rohlhill J, Sandoval NR, Papoutsakis ET. Sort-Seq approach to engineering a formaldehyde-inducible promoter for dynamically regulated *Escherichia coli* growth on methanol. ACS Synth Biol 2017;6(8):1584–95. https://doi.org/10.1021/acssynbio.7b00114.
[24] Woolston BM, Roth T, Kohale I, Liu DR, Stephanopoulos G. Development of a formaldehyde biosensor with application to synthetic methylotrophy. Biotechnol Bioeng 2018;115(1):206–15. https://doi.org/10.1002/bit.26455.
[25] Lee JY, Sung BH, Oh SH, Kwon KK, Lee H, Kim H, et al. C1 compound biosensors: design, functional study, and applications. Int J Mol Sci 2019;20(9):2253. https://doi.org/10.3390/ijms20092253.
[26] Wang H, Gunsalus RP. Coordinate regulation of the *Escherichia coli* formate dehydrogenase *fdnGHI* and *fdhF* Genes in response to nitrate, nitrite, and formate: roles for NarL and NarP. J Bacteriol 2003;185(17):5076–85. https://doi.org/10.1128/jb.185.17.5076-5085.2003.
[27] Zhu R, Zhang G, Jing M, Han Y, Li J, Zhao J, et al. Genetically encoded formaldehyde sensors inspired by a protein intra-helical crosslinking reaction. Nat Commun 2021;12(1):581. https://doi.org/10.1038/s41467-020-20754-4.
[28] Nash T. The colorimetric estimation of formaldehyde by means of the hantzsch reaction. J Biol Chem 1953;55(3):416–21. https://doi.org/10.1042/bj0550416.
[29] Kleeberg U, Klinger W. Sensitive formaldehyde determination with Nash's reagent and a 'Tryptophan reaction'. J Pharmacol Methods 1982;8(1):19–31. https://doi.org/10.1016/0160-5402(82)90004-3.
[30] Le TK, Ju SB, Lee HW, Lee JY, Oh SH, Kwon KK, et al. Biosensor-based directed evolution of methanol dehydrogenase from *Lysinibacillus xylanilyticus*. Int J Mol Sci 2021;22(3):1471. https://doi.org/10.3390/ijms22031471.
[31] Roth TB, Woolston BM, Stephanopoulos G, Liu DR. Phage-assisted evolution of *Bacillus methanolicus* methanol dehydrogenase 2. ACS Synth Biol 2019;8(4):796–806. https://doi.org/10.1021/acssynbio.8b00481.
[32] Becskei A, Serrano L. Engineering stability in gene networks by autoregulation. Nature 2000;405(6786):590–3. https://doi.org/10.1038/35014651.
[33] Osman D, Piergentili C, Chen J, Sayer LN, Uson I, Huggins TG, et al. The effectors and sensory sites of formaldehyde-responsive regulator FrmR and metal-sensing variant. J Biol Chem 2016;291(37):19502–16. https://doi.org/10.1074/jbc.M116.745174.
[34] Denby KJ, Iwig J, Bisson C, Westwood J, Rolfe MD, Sedelnikova SE, et al. The mechanism of a formaldehyde-sensing transcriptional regulator. Sci Rep 2016;6:38879. https://doi.org/10.1038/srep38879.
[35] Guo X, Feng Y, Wang X, Liu Y, Liu W, Li Q, et al. Characterization of the substrate scope of an alcohol dehydrogenase commonly used as methanol dehydrogenase. Bioorg Med Chem Lett 2019;29(12):1446–9. https://doi.org/10.1016/j.bmcl.2019.04.025.
[36] Jumper J, Evans R, Pritzel A, Green T, Figurnov M, Ronneberger O, et al. Highly accurate protein structure prediction with AlphaFold. Nature 2021;596(7873):583–9. https://doi.org/10.1038/s41586-021-03819-2.
[37] Gregory GJ, Bennett RK, Papoutsakis ET. Recent advances toward the bioconversion of methane and methanol in synthetic methylotrophs. Metab Eng 2022;71:99–116. https://doi.org/10.1016/j.ymben.2021.09.005.
[38] Antoniewicz MR. Synthetic methylotrophy: strategies to assimilate methanol for growth and chemicals production. Curr Opin Biotechnol 2019;59:165–74. https://doi.org/10.1016/j.copbio.2019.07.001.
[39] Qin Y, Wu L, Wang J, Han R, Shen J, Wang J, et al. A fluorescence-activated single-droplet dispenser for high accuracy single-droplet and single-cell sorting and dispensing. Anal Chem 2019;91(10):6815–9. https://doi.org/10.1021/acs.analchem.9b01017.
[40] Xiong D, Lu S, Wu J, Liang C, Wang W, Wang W, et al. Improving key enzyme activity in phenylpropanoid pathway with a designed biosensor. Metab Eng 2017;40:115–23. https://doi.org/10.1016/j.ymben.2017.01.006.
[41] Stella RG, Gertzen CGW, Smits SHJ, Gatgens C, Polen T, Noack S, et al. Biosensor-based growth-coupling and spatial separation as an evolution strategy to improve small molecule production of *Corynebacterium glutamicum*. Metab Eng 2021;68:162–73. https://doi.org/10.1016/j.ymben.2021.10.003.